Effect of annealing treatment on microstructures and properties of austenite-based Fe-28Mn-9Al-0.8C lightweight steel with addition of Cu

Zhuo Chen, Ming-xiang Liu, Jian-kang Zhang, Lei Yang, Yun-hu Zhang, *Chang-jiang Song, Qi-jie Zhai

Center for Advanced Solidification Technology (CAST), School of Materials Science and Engineering, Shanghai University, Shanghai 200444, China

Abstract: The mechanical properties of an austenite-based Fe-Mn-Al-C lightweight steel were improved by co-precipitation of nanoscale Cu-rich and κ-carbide particles. The Fe-28Mn-9Al-0.8C-(0,3)Cu (wt.%) strips were near-rapidly solidified and annealed in the temperature range from 500 °C to 700 °C. The microstructure evolution and mechanical properties of the steel under different annealing processes were studied. Microstructural analysis reveals that nanoscale κ-carbides and Cu-rich particles precipitate in the austenite and ferrite of the steel in this annealing temperature range. Co-precipitation of nanoscale Cu-rich particles and κ-carbides provides an obvious increment in the yield strength. At the annealing temperature of 600 °C, both the yield strength and ultimate tensile strength of Fe-28Mn-9Al-0.8C-3Cu (wt.%) steel strip are the highest. The total elongation is 25%, which is obviously higher than that of Cu-free steel strips, for the addition of Cu reduces the large sized κ-carbides precipitated along austenite/ferrite interfaces. When the annealing temperature rises to 700 °C, the strength and ductility of the two steel strips deteriorate due to the formation of massive intergranular κ-carbides precipitated along austenite/ferrite interfaces. It can be concluded that a proper co-precipitation of Cu-rich particles and κ-carbides would improve the properties of austenite-based Fe-Mn-Al-C steel.

Key words: austenite-based steel; Cu-rich particle; near-rapid solidification; co-precipitation strengthening; annealing treatment

CLC numbers: TG142.25　　　　Document code: A　　　　Article ID: 1672-6421(2021)03-207-10

1 Introduction

Fe-Mn-Al-C steels have a great application potential in the automotive industry due to their good ductility and formability, low density and attractive mechanical properties [1-7]. They are mainly used in the structural parts of automobile body to reduce the weight of the automobile [8-10]. Austenite-based Fe-Mn-Al-C steels have high ultimate tensile strength (700–1,100 MPa), which is superior to ferrite-based Fe-Mn-Al-C steels (< 900 MPa), and total elongation can reach 60%. The density can also be reduced to 6.7–7.0 g·cm^{-3}. However, the yield strength of austenite-based Fe-Mn-Al-C steels is low (360–540 MPa) [11-16], which restricts the application of austenite-based Fe-Mn-Al-C steels. Therefore, the yield strength of austenite-based Fe-Mn-Al-C steels needs to be further improved. Precipitation of κ-carbide particles in these steels can effectively improve the yield strength, but the strengthening effect of κ-carbides is not enough in many cases due to its low hardening ability, especially for austenitic Fe-Mn-Al-C lightweight steel with high Mn [17-20].

Cu is often used to enhance the strength of steels through the formation of nanoscale Cu-rich particles in the matrix, and it can improve the properties of cold formability and corrosion resistance [21-28]. Compared with Mo, Ni, V and Nb, which are usually added into Fe-Mn-Al-C steel to achieve precipitation strengthening, the cost of Cu is relatively lower. The precipitation strengthening of Cu-rich particles has been widely studied [29-33]. For example, Ren et al. [21] reported that fine dispersed Cu-rich particles precipitated in a super 304H steel led to an significant increase of hardness. Xi et al. [32] obtained a 316L stainless steel with high strength and good ductility by the precipitation of nanoscale Cu-rich precipitates.

*Chang-jiang Song

Ph.D., Professor. His research interests mainly focus on metal theory and microstructure control, and super performance metastable engineering materials through solidification process control. He has supervised over 20 projects and published more than 100 papers in international journals.

E-mail: riversong@shu.edu.cn; riversxiao@163.com

Combining the precipitation of Cu-rich particles and another type of precipitate usually achieves a better effect in increasing strength of steel [34-37]. Jiao et al. [35] reported an ultra-high strength steel achieved by co-precipitation of nanoscale NiAl and Cu particles, whose tensile strength reached 1.9 GPa. Li et al. [37] obtained another ultra-high strength steel by nanoscale Cu and Ni_3Al particles strengthening. Therefore, in this study, a method to improve the strength of austenitic-based Fe-Mn-Al-C lightweight steels by co-precipitation of Cu-rich particles and κ-carbides is proposed.

Previous studies [38-42] showed that near net-shape method under near-rapid solidification conditions is a simple method to produce Fe-Mn-Al-C steel strips with high properties. So, a centrifugal casting method was used to directly produce the strips in this work. A proper annealing treatment for Fe-Mn-Al-C steels can promote the precipitation of intragranular κ-carbide in austenite and B_2 or DO_3 phase in ferrite, so that the alloy can achieve better mechanical properties. The conventional annealing temperature of Fe-Mn-Al-C steels is between 450 °C–700 °C [2,14,42]. The effect of annealing temperature on the microstructures and properties of the Fe-28Mn-9Al-0.8C-(0,3)Cu (wt.%) lightweight steels was examined.

2 Experimental procedure

The nominal compositions of the studied steels are Fe-28Mn-9Al-0.8C-(0, 3)Cu (wt.%), which are named as 0Cu and 3Cu steel, respectively. The strips were prepared by a centrifugal casting equipment, as shown in Fig. 1 [43]. Firstly, the ingots were prepared using a vacuum induction furnace in Ar atmosphere. Then the ingots were remelted by an induction coil of the centrifugal casting equipment, and the melt flowed into a copper mould which rotated at a speed of 600 r·min⁻¹. The size of the obtained strips is 75 mm × 60 mm × 2.5 mm, and the maximum cooling rate was about $5×10^3$ K·s⁻¹ [44]. Some strips were annealed at 500 °C, 600 °C, 700 °C for 3 h by a tubular vacuum furnace (at a vacuum of 10^{-4} Pa), and then furnace cooling to room temperature. The chemical compositions of the strips were measured by using inductively coupled plasma-atomic emission spectrometry (ICP-AES), and the results are shown in Table 1.

The microstructures of the strips were examined by using a scanning electron microscope (SEM, Hitachi SU-1500, Japan) after mechanical polishing and chemical etching at 70 °C for 30 s in a mixed solution of supersaturated picric acid (94 mL), 10%
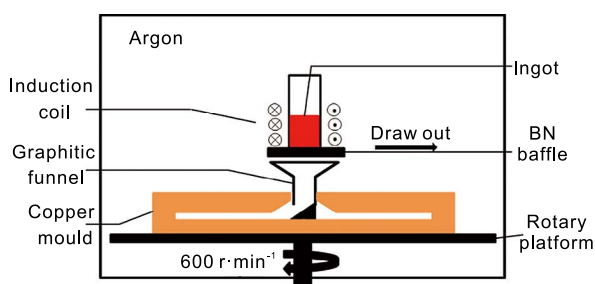
Table 1: Measured composition of two strips (wt.%)

Steel	Mn	Al	C	Cu	Fe
0Cu	27.88	8.10	0.84	0	Bal.
3Cu	26.67	8.41	0.81	2.82	Bal.

hydrochloric acid (3 mL) and dodecyl benzene sulfonic acid (3 mL). X-ray diffraction (XRD, Rigaku D/max-2200×, Cu Kα target operated at 40 kV and 60 mA) and transmission electron microscope (TEM, JEM-2010F operated at 200 kV, Japan) were used to identify the phases in the strips. TEM specimens were mechanically polished to a thickness of 50 μm, cut into a 3 mm-diameter disc and thinned by twin-jet electropolishing in a solution of 10vol.% perchloric acid+90vol.% ethyl alcohol at −28 °C to −32 °C with a voltage of 40 V. Tensile tests were conducted at a strain rate of 10^{-3} s⁻¹ at room temperature by using MTS Criterion Model 44 with 10 kN capacity. The size of the tensile specimens is 4 mm in guage width and 12 mm in guage length, and at least three specimens were tested for each steel.

3 Results

3.1 Microstructure of strips

Figure 2 shows the phases of 0Cu and 3Cu steel strips determined by XRD. It can be seen that austenite and ferrite are the main phases in all the strips. The phase constituents of a steel strip annealed at 500 °C for 3 h have no obvious change compared with the as-cast strip. However, when the annealing temperature is raised, especially at 700 °C, the diffraction peaks at position of $2\theta = 41.44°/48.24°$ corresponding to κ-carbide are detected in both strips. This indicates that the precipitation of κ-carbide is promoted by annealing.

Figure 3 shows SEM images of 0Cu and 3Cu strips in different conditions. Similar to the as-cast strip, the ferrite in 3Cu strip annealed at 500 °C shows a fine banded shape [Fig. 3(f)], whereas massive irregular bulk ferrite exists in 0Cu strips [Fig. 3(b)]. As the annealing temperature increases to 600 °C, the content of ferrite in the 0Cu and 3Cu samples is increased, but its size is slightly decreased. A black precipitated phase is observed in the ferrite near the phase boundary in the Cu-free strip [Fig. 3(c)], which is not observed in 3Cu strips [Fig. 3(g)]. As the annealing temperature further increases to 700 °C, the black precipitated particles appear in the ferrite of both strips, and their size becomes greater.

SEM observation in high magnification and EDS analysis were carried out on the strips annealed at 600 °C for 3 h. The results are shown in Fig. 4. It is found from Fig. 4(a) that a great number of black elongated or granular particles precipitate in the 0Cu strip, but few particles are observed in the 3Cu strip [Fig. 4(b)]. According to the energy spectrum analysis, the content of Mn and C in the precipitated phase is significantly high, as shown in Fig. 4(c). According to the literature [33], when the annealing temperature exceeds 550 °C, a part of austenite
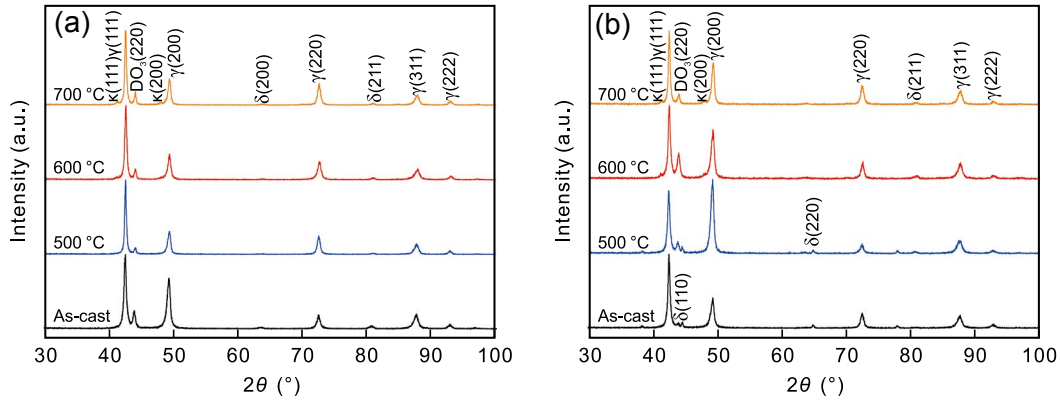

Fig. 1: Schematic illustration of centrifugal casting equipment [43]

Fig. 2: X-ray diffraction patterns of steel strips: (a) 0Cu; (b) 3Cu
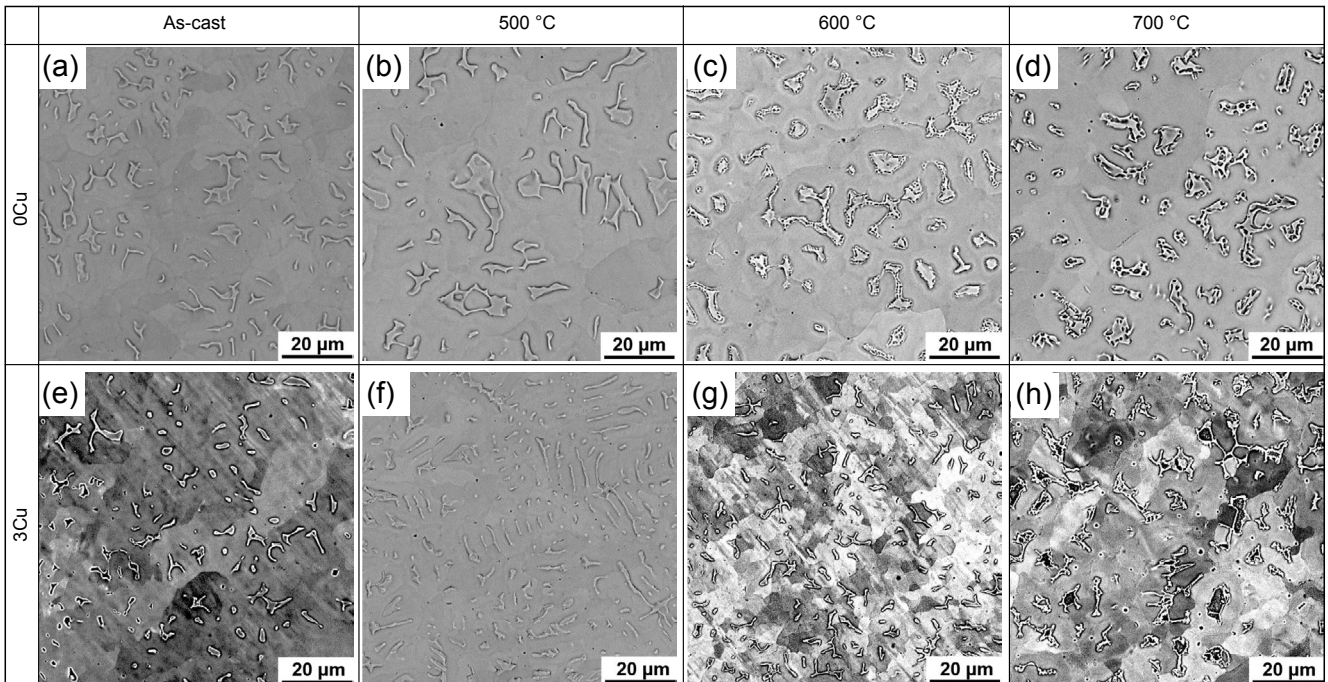

Fig. 3: Microstructures of 0Cu and 3Cu strips. 0Cu: (a) as-cast; (b) 500 °C; (c) 600 °C; (d) 700 °C; 3Cu: (e) as-cast; (f) 500 °C; (g) 600 °C; (h) 700 °C
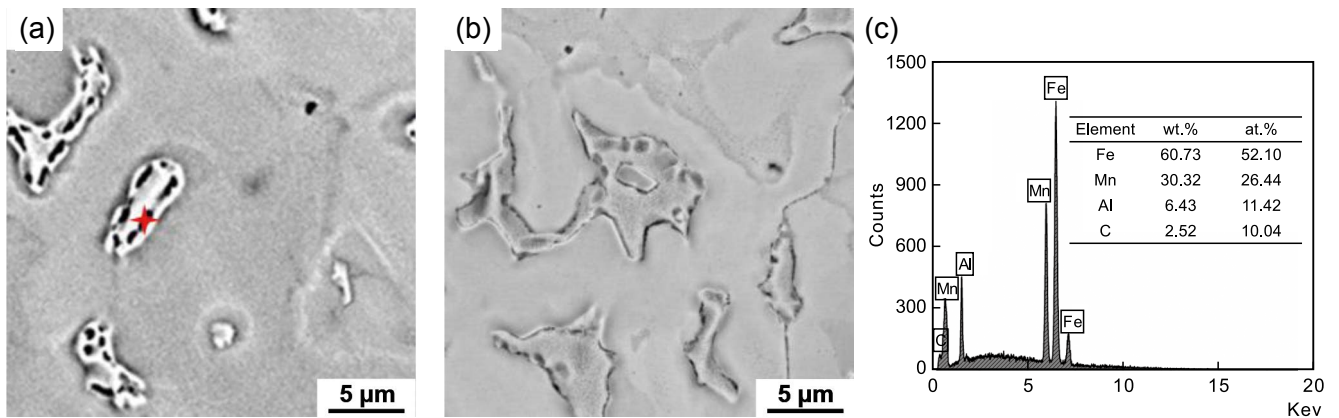

Element	wt.%	at.%
Fe	60.73	52.10
Mn	30.32	26.44
Al	6.43	11.42
C	2.52	10.04

Fig. 4: High magnification SEM images of strips annealed at 600 °C: (a) 0Cu; (b) 3Cu; (c) EDS analysis of precipitation in (a)

would be transformed into ferrite and intergranular κ-carbide in some austenite matrix lightweight steels, so the black precipitation is determined as κ-carbide. It can be concluded that the addition of 3wt.% Cu reduces the precipitation of κ-carbide along austenite/ferrite interfaces in the strip annealed at 600 °C for 3 h.

3.2 Mechanical properties

Figures 5(a) and (b) show the engineering stress-strain curves of 0Cu and 3Cu steel strips, respectively. The detailed values for the mechanical properties including yield strength (YS), ultimate tensile strength (UTS) and total elongation (TE) are listed in Table 2. Results show that when 3wt.%Cu is added, the YS and UTS of Fe-28Mn-9Al-0.8C as-cast strips are reduced by 30–50 MPa, but its elongation increases slightly. After annealing treatment, the strength of both Cu-containing and Cu-free steel strips increases significantly compared with as-cast steel strip. The increases in YS and UTS of 3Cu steel strip are obviously higher than those of the Cu-free steel strip

[Figs. 5(c) and (d)], which makes YS and UTS of 3Cu strip exceed those of Cu-free strip by 30–70 MPa after annealing at 600 °C for 3 h. However, when the annealing temperature increases to 600 °C, the elongation of Cu-free and Cu-containing strips clearly decreases, which should be ascribed to the greater precipitation of κ-carbide, especially the appearance of κ-carbide at austenite/ferrite interfaces. Moreover, when the annealing temperature reaches to 700 °C, the strength of the two steel strips is also clearly reduced. Generally, the elongation of Cu-containing strips under the same condition is slightly better than that of Cu-free strip except the strips annealed at 700 °C.
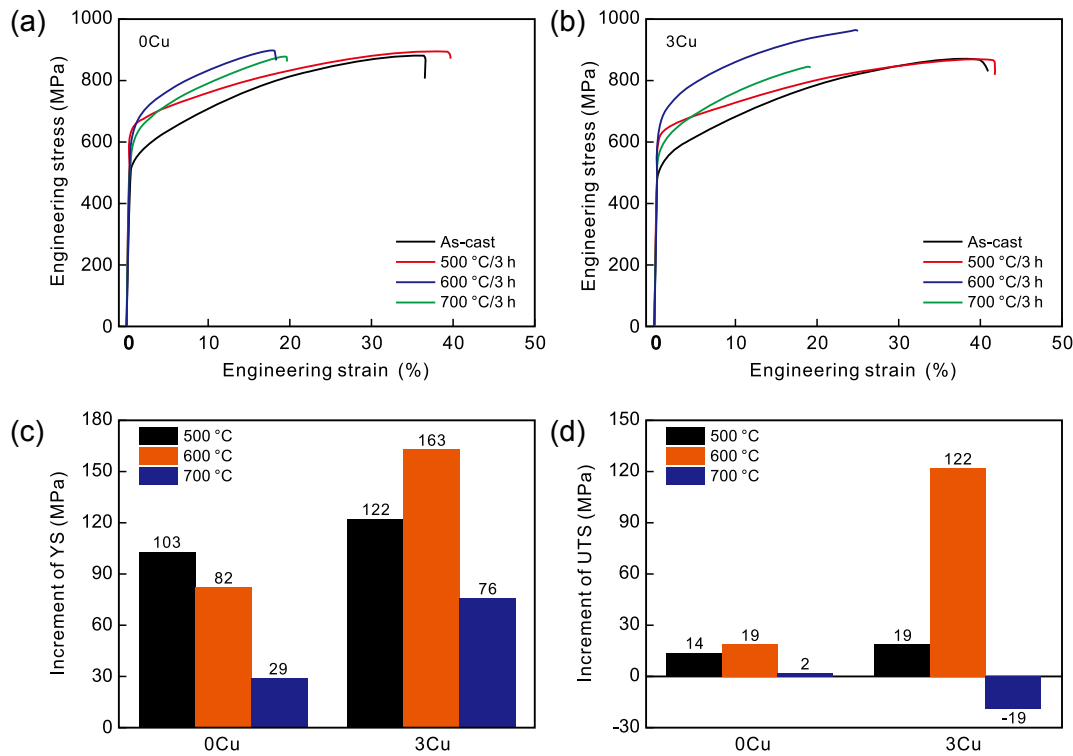

Fig. 5: Engineering stress-strain curves of strips: (a) 0Cu; (b) 3Cu; and increases in strength of annealed strips: (c) YS; (d) UTS

Table 2: Tensile properties of Fe-28Mn-9Al-0.8C-(0,3)Cu strips under different states

Sample state	0Cu			3Cu		
	YS (MPa)	UTS (MPa)	TE (%)	YS (MPa)	UTS (MPa)	TE (%)
As-cast	538±19	877±28	35±3	490±24	843±30	38±6
500 °C/3 h	641±5	891±13	39±3	612±12	862±15	40±5
600 °C/3 h	620±11	896±24	17±3	653±17	965±23	25±6
700 °C/3 h	567±4	879±3	20±1	566±2	824±20	18±4

3.3 TEM analysis of precipitated phases

To well understand the reason for change of the mechanical properties, TEM was performed on the Cu-free and Cu-containing steel strips annealed at 500 °C and 700 °C, respectively.

3.3.1 Strips annealed at 500 °C

Figure 6 shows the microstructures of 0Cu strip after annealing treatment at 500 °C for 3 h. Figure 6(a) is a bright-field (BF) image of austenite. According to a selected-area electron diffraction (SAED) pattern of austenite taken from $[110]_\gamma$ axis,
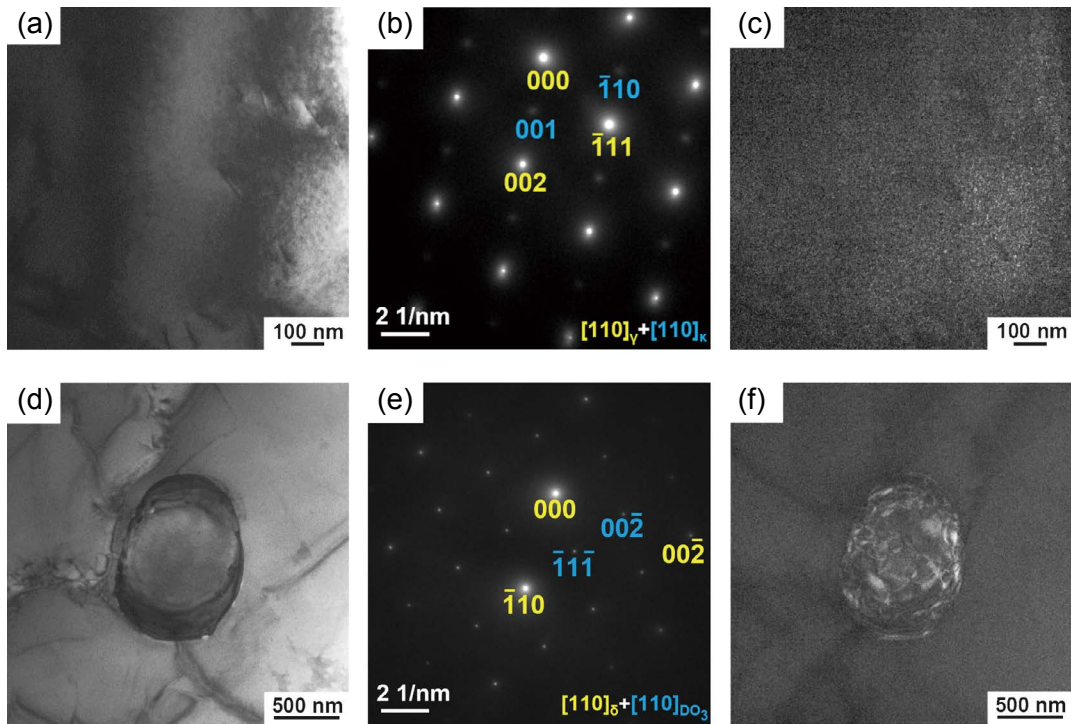
Fig. 6: TEM images of 0Cu steel strip after annealing at 500 °C for 3 h: (a) BF image of austenite; (b) SAED pattern along $[110]_\gamma$ zone axis from (a); (c) DF image of κ-carbide particles; (d) BF image of ferrite; (e) SAED pattern along $[110]_\delta$ zone axis from (d); (f) DF image of DO_3 phase

a superlattice belonging to κ-carbide is found [Fig. 6(b)]. The dark-field (DF) image [Fig. 6(c)] also indicates that there are some nanoscale κ-carbides in the austenite matrix. The SAED pattern taken from the ferrite area along $[110]_\delta$ axis is shown in Fig. 6(e), a diffraction spot belonging to DO_3 phase can be

detected. The corresponding DF image [Fig. 6(f)] illustrates that the scaly DO_3 phase with a size of about 100 nm appears in the ferrite after annealing at 500 °C for 3 h.

Figure 7 shows the TEM image of 3Cu strips annealed at 500 °C for 3 h. A superlattice of κ-carbides also appears in the
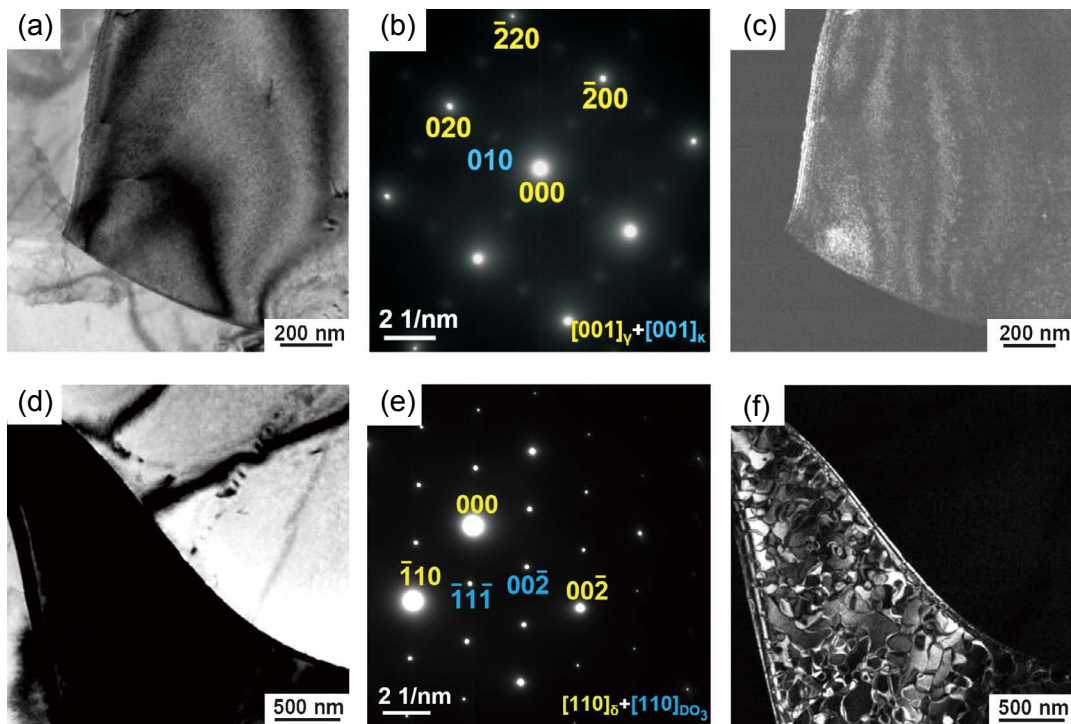

Fig. 7: TEM images of 3Cu steel strip after annealing at 500 °C for 3 h: (a) BF image of austenite; (b) SAED pattern along $[001]_\gamma$ zone axis from (a); (c) DF image of κ-carbide particles; (d) BF image of ferrite; (e) SAED pattern along $[110]_\delta$ zone axis from (d); (f) DF image of DO_3 phase

austenitic matrix [Fig. 7(b)], and some granular κ-carbides are dispersedly precipitated in the matrix from the corresponding DF images [Fig. 7(c)]. Figure 7(e) presents SAED pattern of ferrite taken from $[110]_\delta$ axis, which shows there also exists a superlattice corresponding to the ordered DO_3 phase in ferrite. The size and morphology of DO_3 phase are similar to that of Cu-free strips [Fig. 7(f)].

3.3.2 Strips annealed at 700 °C

Figure 8 shows TEM images of 0Cu strips annealed at 700 °C. According to corresponding DF images [Figs. 8(c) and (f)], there are two different morphologies of κ-carbides in austenitic matrix after annealing at 700 °C. Some are granular κ-carbides with size less than 10 nm, the others are large bulk κ-carbides. This suggests that the κ-carbides are significantly coarsening after annealing at 700 °C. From the SAED pattern of ferrite taken from $[110]_\delta$ axis [Fig. 8(h)], there still exists a superlattice of DO_3

ordered phase, and its dark field image is shown in Fig. 8(i).

Figure 9 presents the TEM images of 3Cu strips annealed at 700 °C for 3 h. It is found that the size of κ-carbides in austenite is also greater than those of strips annealed at 500 °C, but fewer large-bulk shape κ-carbides are found in 3Cu strips after annealing at 700 °C, as shown in Figs. 9(a) and (c), indicating that the addition of 3wt.% Cu reduces the precipitation of coarse κ-carbides with bulk shape. Figures 9(d) and (f) show the BF and DF images of ferrite, respectively. It can be seen that the DO_3 phase in ferrite presents a water ripple shape and becomes larger compared to that of 3Cu strips annealed at 500 °C.

3.4 EPMA analysis of Cu precipitates

The diffraction belonging to Cu precipitates is not found in the SAED pattern of austenite. Therefore, EPMA was used to analyze the distribution of Cu element in the 3Cu steel strip and the results are shown in Fig. 10.
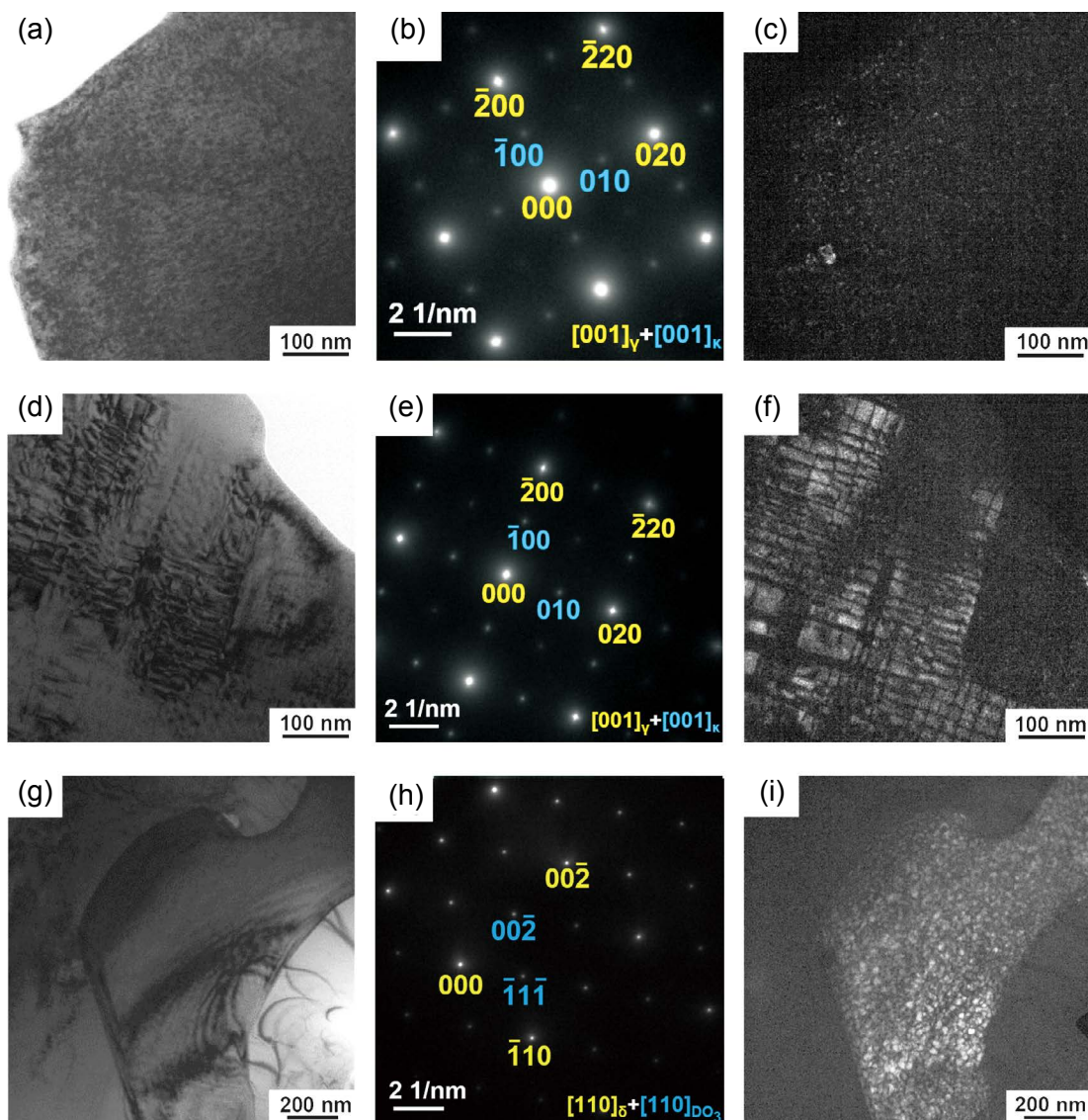

Fig. 8: TEM images of 0Cu steel strip after annealing at 700 °C for 3 h: (a) BF image of austenite; (b) SAED pattern along $[001]_\gamma$ zone axis from (a); (c) DF image of κ-carbide particles; (d) BF image of austenite; (e) SAED pattern along $[001]_\gamma$ zone axis from (d); (f) DF image of κ-carbide particles; (g) BF image of ferrite; (h) SAED pattern along $[110]_\delta$ zone axis from (g); (i) DF image of DO_3 phase
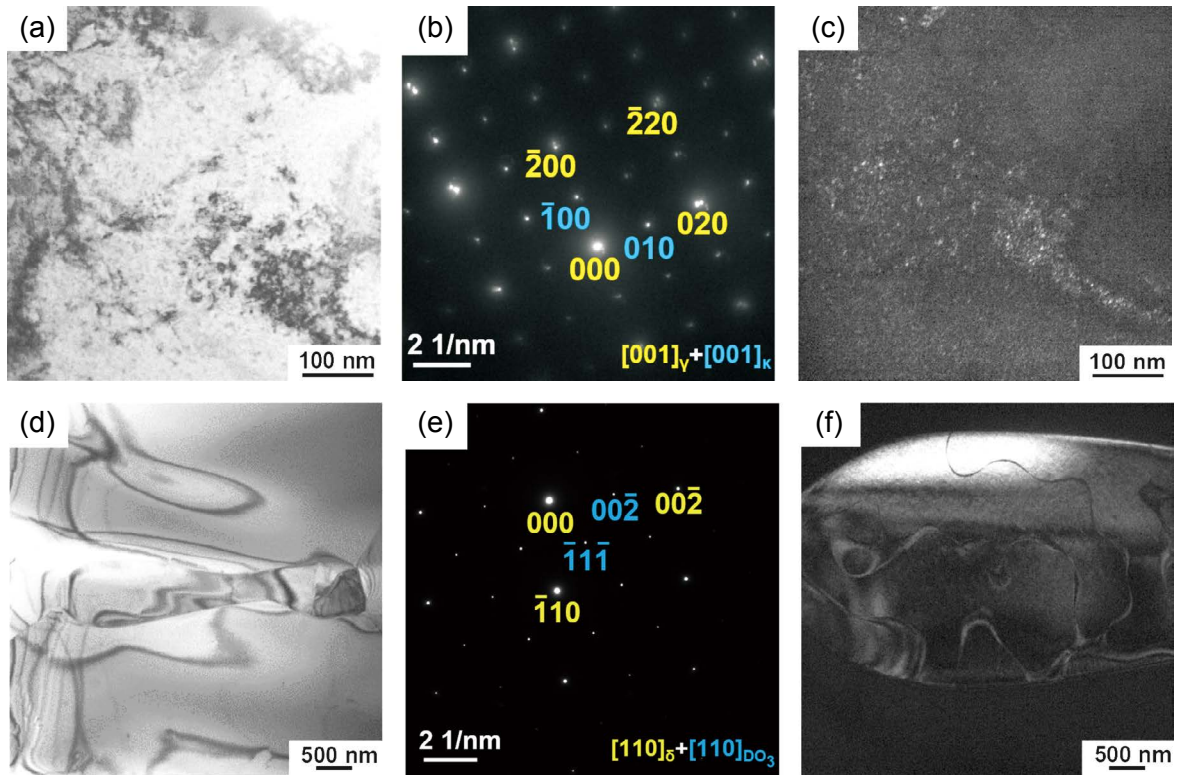
Fig. 9: TEM images of 3Cu steel strip after 700 °C for 3 h: (a) BF image of austenite; (b) SAED pattern along [001]$_\gamma$ zone axis from (a); (c) DF image of κ-carbide particles; (d) BF image of ferrite; (e) SAED pattern along [110]$_\delta$ zone axis from (d); (f) DF image of DO$_3$ phase
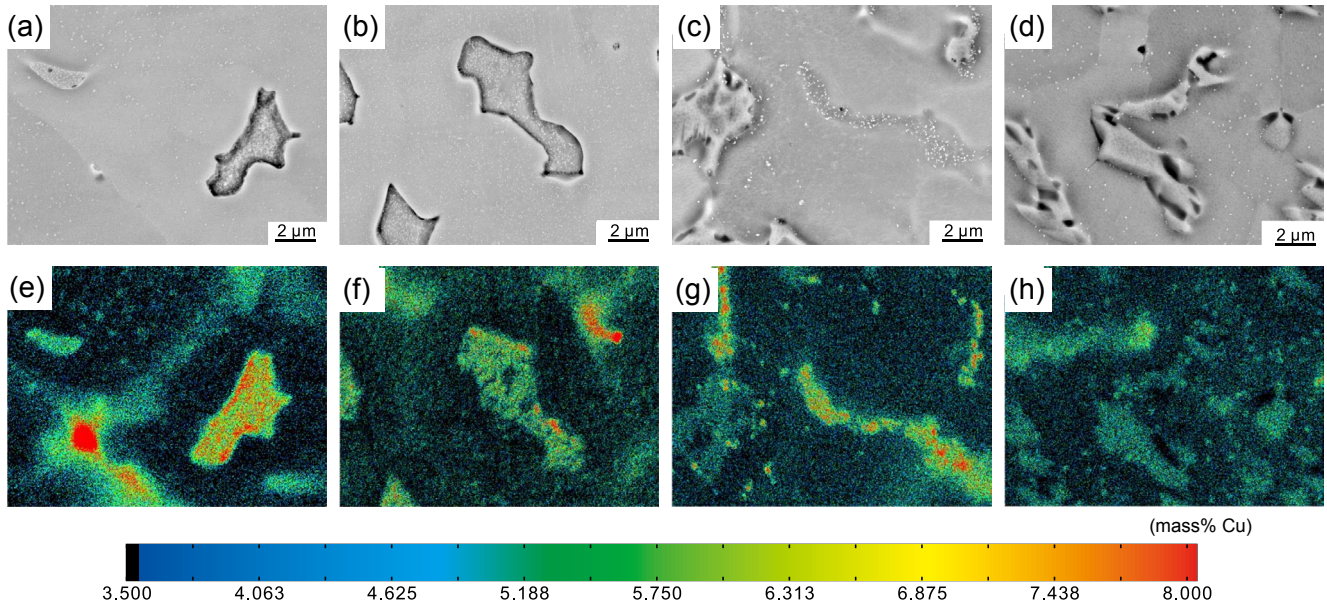

Fig. 10: EPMA images of 3Cu strips: (a) and (e) as-cast; (b) and (f) annealed at 500 °C; (c) and (g) annealed at 600 °C; (d) and (h) annealed at 700 °C

The results of EPMA mapping show that there are some large Cr-rich regions with high Cu content at the grain/phase boundary and inside the ferrite, and some small Cu-rich regions with slightly high Cu content in the austenite matrix. As the annealing temperature increases, the size and number of large Cu-rich regions gradually decrease, while the number of small Cu-rich regions in austenite increases.

To further examine these small Cu-rich regions, a TEM equipped with energy dispersive spectrometer (TEM-EDS) was used to detect these regions in a 3Cu steel strip annealed at 500 °C for 6 h (a longer annealing time to obtain more Cu-rich precipitates). It can be found there are a lot of Cu-rich particles [black regions in Fig. 11(a)] in the austenite matrix, and the average size of these particles is about 45 nm. Thus it is determined that co-precipitation of nano-scale Cu-rich and κ-carbide particles is achieved in the 3Cu strips annealed at 500 °C.
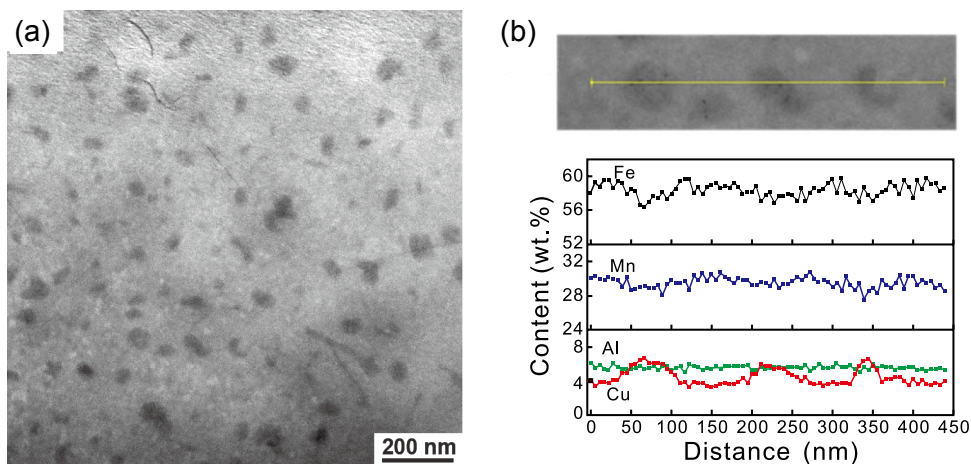
Fig. 11: TEM-EDS of 3Cu steel strip annealed at 500 °C for 6 h: (a) mapping; (b) line scanning

4 Discussion

An addition of 3wt.% Cu decreases the yield strength of the strip in the as-cast condition due to an increase of austenite volume fraction. Austenite as a soft phase leads to the decrease in strength [45]. Moreover, Cu addition also causes the increase of stacking fault energy for austenite-based lightweight steels [46,47]. The increase in stacking fault energy would reduce the width of extended dislocations which is in favor of the climbing, cross-slip and mutual cutting of dislocations [46]. Therefore, the increase of austenite content and stacking fault energy of austenite matrix reduces the yield strength of 3Cu steel strip. After annealing, the increase in the strength of 3Cu steel strip is obvious. Under near-rapid solidification condition, interstitial carbon atom and substitutional Cu atom can be supersaturated in austenite and ferrite [42], which means that δ ferrite and γ austenite are metastable. Thus, the formation of nanoscale κ-carbides and Cu-rich particles can be promoted during annealing treatment. Meanwhile, the increasing temperature can provide more thermodynamic driving force for precipitation of Cu-rich particles and accelerate the formation of these particles [32], and at the same time, other atoms are rejected from Cu-rich particles resulting in an enrichment of these elements [48,49]. Thus, the formation of Cu-rich particles could promote the precipitation of κ-carbides, and the co-precipitation of κ-carbides and Cu-rich particles provides higher strengthening effect on the strength of 3Cu steel strip. When the annealing temperature reaches 700 °C, the strength and total elongation of the two steel strips are decreased, which resulted by the formation of a large number of coarse κ-carbides and intergranular κ-carbides around phase boundaries. In addition, the solubility of Cu increases when the temperature rises [50], which can reduce the number of Cu-rich precipitates. The strengthening effect is weakened, leading to a decline in the strength of the steel.

The total elongation of two steel strips annealed at 500 °C increases compared with the as-cast steel strip. The reason should be a release of thermal stress after annealing treatment [51]. When annealing temperature increases, the precipitation of intergranular κ-carbides around phase boundary can result in crack initiation and propagation, which makes total elongation of the strips decrease significantly [52,53]. Compared with the Cu-free steel strip, the total elongation of the Cu-containing steel strip annealed at 600 °C is much higher. This is because the addition of 3wt.% Cu reduces the precipitation of intergranular κ-carbides in the steel strips annealed at 600 °C.

5 Conclusions

This work mainly studied the effect of annealing temperature on the microstructures and mechanical properties of Fe-28Mn-9Al-0.8C-(0,3)Cu (wt.%) steel, an austenite-based lightweight steel strengthened by co-precipitation of κ-carbides and Cu-rich particles, prepared under near rapid solidification. The conclusions are obtained as follows:

(1) The near-rapidly solidified Fe-28Mn-9Al-0.8C-(0,3)Cu lightweight steel strips mainly contain (γ+δ) duplex phases. Annealing at 500 °C–700 °C for 3 h can promote the precipitation of κ-carbides in the γ matrix of Cu-free steel strip and achieve co-precipitation of nanoscale Cu-rich particles and κ-carbides in the Cu-containing steel strip. Co-precipitation of Cu-rich particles and κ-carbides provides a high increment in yield strength.

(2) Annealing at 500 °C makes yield strength of Cu-free and Cu-containing steels significantly increase, and simultaneously slightly improves their ductility. A large number of intergranular κ-carbides along austenite/ferrite interfaces are formed in Cu-free steel strips annealed at 600 °C, which make its total elongation obviously decrease. An addition of 3wt.% Cu inhibits the formation of the intergranular κ-carbides in Cu-containing steel strip annealed at 600 °C, causing a further increase in strength and small decrease in total elongation. The yield strength, ultimate tensile strength and total elongation of the Cu-containing steel strip annealed at 600 °C are 653 MPa, 965 MPa and 25%, respectively, which are higher than those of Cu-free steel strip. Both strength and ductility of the two steel strips annealed at 700 °C obviously decrease due to the formation of more intergranular κ-carbides.

Acknowledgements

References

[1] Kim S H, Kim H, Kim N J. Brittle intermetallic compound makes ultrastrong low-density steel with large ductility. Nature, 2015, 518(7537): 77−85.

[2] Choi K, Seo C H, Lee H, et al. Effect of aging on the microstructure and deformation behavior of austenite base lightweight Fe-28Mn-9Al-0.8C steel. Scripta Mater., 2010, 63(10): 1028−1031.

[3] Zhang L F, Song R B, Zhao C, et al. Evolution of the microstructure and mechanical properties of an austenite-ferrite Fe-Mn-Al-C steel. Mater. Sci. Eng. A, 2015, 643: 183−193.

[4] Yoo J D, Hwang S W, Park K T. Factors influencing the tensile behavior of a Fe-28Mn-9Al-0.8C steel. Mater. Sci. Eng. A, 2009, 508(1−2): 234−240.

[5] Sutou Y, Kamiya N, Umino R, et al. High-strength Fe-20Mn-Al-C-based alloys with low density. ISIJ Int., 2010, 50(6): 893−899.

[6] Hwang S W, Ji J H, Lee E G, et al. Tensile deformation of a duplex Fe-20Mn-9Al-0.6C steel having the reduced specific weight. Mater. Sci. Eng. A, 2011, 528(15): 5196−5203.

[7] Ha M C, Koo J M, Lee J K, et al. Tensile deformation of a low density Fe-27Mn-12Al-0.8C duplex steel in association with ordered phases at ambient temperature. Mater. Sci. Eng. A, 2013, 586: 276−283.

[8] Frommeyer G, Brux U. Microstructures and mechanical properties of high-strength Fe-Mn-Al-C light-weight TRIPLEX steels. Steel Res. Int., 2006, 77(9−10): 627−633.

[9] Schulte A. Quality improvements of cast lightweight steel P900 armor. Int. J. Met., 2010, 4(1): 59−63.

[10] Zambrano O A. A general perspective of Fe-Mn-Al-C steels. J. Mater. Sci., 2018, 53(20): 14003−14062.

[11] Yoo J D, Hwang S W, Park K T. Origin of extended tensile ductility of a Fe-28Mn-10Al-1C steel. Metall. Mater. Trans. A, 2009, 40(7): 1520−1523.

[12] Lee K, Park S J, Moon J, et al. β-Mn formation and aging effect on the fracture behavior of high-Mn low-density steels. Scripta Mater., 2016, 124: 193−197.

[13] Xing J, Hou L F, Du H Y, et al. Effects of pre-deformation on the kinetics of β-Mn phase precipitation and mechanical properties in Fe-30Mn-9Al-1C lightweight steel. Metal Mater. Trans. A, 2019, 50(6): 2629−2639.

[14] Feng Y F, Song R B, Pei Z Z, et al. Effect of aging isothermal time on the microstructure and room-temperature impact toughness of Fe-24.8Mn-7.3Al-1.2C austenitic steel with κ-carbides precipitation. Met. Mater. Int., 2018, 24(5): 1012−1023.

[15] Yoo J D, Park K T. Microband-induced plasticity in a high Mn-Al-C light steel. Mater. Sci. Eng. A, 2008, 496(1−2): 417−424.

[16] Yoo J, Kim B, Park Y, et al. Microstructural evolution and solidification cracking susceptibility of Fe-18Mn-0.6C-xAl steel welds. J. Mater. Sci., 2015, 50(1): 279−286.

[17] Song W, Zhang W, Appen J V, et al. κ-phase formation in Fe-Mn-Al-C austenitic steels. Steel Res. Int., 2015, 86(10): 1161−1169.

[18] Park K T, Hwang S W, Son C Y, et al. Effects of heat treatment on microstructure and tensile properties of a Fe-27Mn-12Al-0.8C low-density steel. JOM, 2014, 66(9): 1828−1836.

[19] Chang K M, Chao C G, Liu T F. Excellent combination of strength and ductility in an Fe-9Al-28Mn-1.8C alloy. Scr. Mater., 2010, 63(2): 162−165.

[20] He W, Wang B L, Yang Y, et al. Microstructure and mechanical behavior of a low-density Fe-12Mn-9Al-1.2C steel prepared using centrifugal casting under near-rapid solidification. J. Iron Steel Res. Int., 2018, 25(8): 830−838.

[21] Ren L, Nan L, Yang K. Study of copper precipitation behavior in a Cu-bearing austenitic antibacterial stainless steel. Mater. Des., 2011, 32(4): 2374−2379.

[22] Ren L, Zhu J M, Nan L, et al. Differential scanning calorimetry analysis on Cu precipitation in a high Cu austenitic stainless steel. Mater. Des., 2011, 32(7): 3980−3985.

[23] Tan S P, Wang Z H, Cheng S C, et al. Effect of Cu content on aging precipitation behaviors of Cu-rich phase in Fe-Cr-Ni alloy. J. Iron Steel Res. Int., 2010, 17(5): 63−68.

[24] Sen I, Amankwah E, Kumar N S, et al. Microstructure and mechanical properties of annealed SUS 304H austenitic stainless steel with copper. Mater. Sci. Eng. A, 2011, 528(13−14): 4491−4499.

[25] Gaber A, Ali A M, Matsuda K, et al. Study of the developed precipitates in Al-0.63Mg-0.37Si-0.5Cu (wt.%) alloy by using DSC and TEM techniques. J. Alloy. Compd., 2007, 432(1−2): 149−155.

[26] Deschamps A, Militzer M, Poole W J. Precipitation kinetics and strengthening of a Fe-0.8wt.% Cu alloy. ISIJ Int., 2001, 41(2): 196−205.

[27] Bhagat A N, Pabi S K, Ranganathan S, et al. Aging behaviour in copper bearing high strength low alloy steels. ISIJ Int., 2004, 44(1): 115−122.

[28] Rana R, Bleck W, Singh S B, et al. Development of high strength interstitial free steel by copper precipitation hardening. Mater. Lett., 2007, 61(14−15): 2919−2922.

[29] Jain D, Isheim D, Hunter A H, et al. Multicomponent high-strength low-alloy steel precipitation-strengthened by sub-nanometric Cu precipitates and M₂C carbides. Metall. Mater. Trans. A, 2016, 47(8): 3860−3872.

[30] Dhua S K, Mukerjee D, Sarma D S. Influence of tempering on the microstructure and mechanical properties of HSLA-100 steel plates. Metall. Mater. Trans. A, 2001, 32(9): 2259−2270.

[31] Dhua S K, Mukerjee D, Sarma D S. Influence of thermomechanical treatments on the microstructure and mechanical properties of HSLA-100 steel plates. Metall. Mater. Trans. A, 2003, 34(2): 241−253.

[32] Xi T, Shahzad M B, Xu D, et al. Copper precipitation behavior and mechanical properties of Cu-bearing 316L austenitic stainless steel: A comprehensive cross-correlation study. Mater. Sci. Eng. A, 2016, 675: 243−252.

[33] Xi T, Shahzad M B, Xu D, et al. Effect of copper addition on mechanical properties, corrosion resistance and antibacterial property of 316L stainless steel. Mater. Sci. Eng. C-Biomimetic Supramol. Syst., 2017, 71: 1079−1085.

[34] Jiao Z B, Luan J H, Zhang Z W, et al. Synergistic effects of Cu and Ni on nanoscale precipitation and mechanical properties of high-strength steels. Acta Mater., 2013, 61(16): 5996−6005.

[35] Jiao Z B, Luan J H, Miller M K, et al. Precipitation mechanism and mechanical properties of an ultra-high strength steel hardened by nanoscale NiAl and Cu particles. Acta Mater., 2015, 97: 58−67.

[36] Kapoor M, Isheim D, Ghosh G, et al. Aging characteristics and mechanical properties of 1600 MPa body-centered cubic Cu and B2-NiAl precipitation-strengthened ferritic steel. Acta Mater., 2014, 73: 56−74.

[37] Li Z H, Chai F, Yang L, et al. Mechanical properties and nanoparticles precipitation behavior of multi-component ultra high strength steel. Mater. Des., 2020, 191: 108637.

[38] Song C J, Xia W B, Zhang J, et al. Microstructure and mechanical properties of Fe-Mn based alloys after sub-rapid solidification. Mater. Des., 2013, 51: 262–267.

[39] Song C J, Lu W, Xie K, et al. Microstructure and mechanical properties of sub-rapidly solidified Fe-18wt%Mn-C alloy strip. Mater. Sci. Eng. A, 2014, 610: 145–153.

[40] Song C J, Yang Y, Guo Y Y, et al. Solidification characteristics of Fe-Ni peritectic alloy thin strips under a near-rapid solidification condition. China Foundry, 2015, 12(3): 189-195.

[41] Zhang J L, Hu C H, Zhang Y H, et al. Microstructures, mechanical properties and deformation of near-rapidly solidified low-density Fe-20Mn-9Al-1.2C-xCr steels. Mater. Des., 2020, 186: 108307.

[42] Liu L B, Li C M, Yang Y, et al. A simple method to produce austenite-based low-density Fe-20Mn-9Al-0.75C steel by a near-rapid solidification process. Mater. Sci. Eng. A, 2017, 679: 282–291.

[43] Yang Y, Zhang J L, Hu C H, et al. Structures and properties of Fe-(8–16) Mn-9Al-0.8 C low density steel made by a centrifugal casting in near-rapid solidification. Mater. Sci. Eng. A, 2019, 748: 74–84.

[44] Yang R, Xia W B, Song C J, et al. Phase formation of Fe-Mn binary alloy during sub-rapid solidification. Adv. Mater. Res., 2012, 391: 741–744.

[45] Chen S P, Rana R, Haldar A, et al. Current state of Fe-Mn-Al-C low density steels. Prog. Mater. Sci., 2017, 89: 345–391.

[46] Ohkubo N, Miyakusu K, Uematsu Y, et al. Effect of alloying elements on the mechanical properties of the stable austenitic stainless steel. ISIJ Int., 1994, 34(9): 764–772.

[47] Dumay A, Chateau J P, Allain S, et al. Influence of addition elements on the stacking-fault energy and mechanical properties of an austenitic Fe-Mn-C steel. Mater. Sci. Eng. A, 2008, 483–484: 184–187.

[48] Mulholland M D, Seidman D N. Nanoscale co-precipitation and mechanical properties of a high-strength low-carbon steel. Acta Mater., 2011, 59(5): 1881–1897.

[49] Jiao Z B, Luan J H, Miller M K, et al. Co-precipitation of nanoscale particles in steels with ultra-high strength for a new era. Mater. Today, 2017, 20(3): 142–154.

[50] Heinze M H. The effect of aging treatment on the microstructure and properties of copper-precipitation strengthened HSLA steel. Master. Thesis, California: Naval Postgraduate School, 1988: 7–8.

[51] Wang X L, Zhang W N, Liu Z Y, et al. Improvement on room-temperature ductility of 6.5 wt.% Si steel by stress-relief annealing treatments after warm rolling. Mater. Charact., 2016, 122: 206–214.

[52] Sohn S S, Lee B J, Lee S, et al. Effects of aluminum content on cracking phenomenon occurring during cold rolling of three ferrite-based lightweight steel. Acta Mater., 2013, 61(15): 5626–5635.

[53] Sohn S S, Lee B J, Lee S, et al. Microstructural analysis of cracking phenomenon occurring during cold rolling of (0.1-0.7) C-3Mn-5Al lightweight steels. Met. Mater. Int., 2015, 21(1): 43–53.